Demonstration of scattering suppression in retardation-based plasmonic nanoantennas

Nielsen, M.G.; Pors, A.; Nielsen, Rasmus Bundgaard; Boltasseva, Alexandra; Albrektsen, O.; Bozhevolnyi, S.I.

Published in:
Optics Express

Link to article, DOI:
10.1364/OE.18.014802

Publication date:
2010

Document Version
Publisher's PDF, also known as Version of record

Demonstration of scattering suppression in retardation-based plasmonic nanoantennas

Michael G. Nielsen,[1,*] Anders Pors,[2] Rasmus B. Nielsen,[3] Alexandra Boltasseva,[3,4] Ole Albrektsen[1] and Sergey I. Bozhevolnyi[1]

[1]*Institute of Sensors, Signals and Electrotechnics, University of Southern Denmark, Niels Bohrs Allé 1, DK-5230 Odense M, Denmark*

[2]*Mads Clausen Institute (MCI), University of Southern Denmark, Alsion 2, DK-6400 Sønderborg, Denmark*

[3]*DTU Fotonik, Technical University of Denmark, Ørsteds Plads, DK-2800 Kongens Lyngby, Denmark*

[4]*School of Electrical and Computer Engineering and Birck Nanotechnology Center, Purdue University, West Lafayette IN, 47907, USA*

**mgni@sense.sdu.dk*

Abstract: Modifications in scattering strength of and local field enhancement by retardation-based plasmonic nanoantennas when being transformed from straight nanorods to split-ring resonators are investigated experimentally. Scattering properties are characterized with linear reflection and extinction spectroscopy of nanoantenna arrays, whereas local field enhancements are evaluated for individual nanoantennas using two-photon-excited photoluminescence (TPL) microscopy. The linear and nonlinear optical characterizations reveal that the optical response of nanoantennas is determined by the interference of counter-propagating short-range surface plasmon polaritons (SR-SPP) and that the transformation of nanorods into split-rings by bending significantly influences the scattering strength. Importantly, strong suppression of scattering for the fundamental SR-SPP resonance is observed when the bend radius is decreased, a feature that is attributed to the decrease in the nanoantenna electric-dipole response when bending the nanorods. The experimental observations are corroborated with numerical simulations using the finite-element method.

OCIS codes: (240.6680) Surface plasmons; (260.3910) Metal optics; (070.5753) Resonators; (290.0290) Scattering; (190.0190) Nonlinear optics; (220.4241) Nanostructure fabrication;

References and links

1. S. A. Maier, *Plasmonics: Fundamentals and Applications, (Springer, New York, 2007).*
2. D. K. Gramotnev, and S. I. Bozhevolnyi, "Plasmonics beyond the diffraction limit," Nat. Photonics **4**(2), 83–91 (2010).
3. K. A. Willets, and R. P. Van Duyne, "Localized surface plasmon resonance spectroscopy and sensing," Annu. Rev. Phys. Chem. **58**(1), 267–297 (2007).
4. M. Pelton, J. Aizpurua, and G. Bryant, "Metal-nanoparticle plasmonics," Laser Photon. Rev. **2**(3), 136–159 (2008).
5. T. Søndergaard, and S. I. Bozhevolnyi, "Slow-plasmon resonant nanostructures: Scattering and field enhancements," Phys. Rev. B **75**(7), 073402 (2007).
6. T. Søndergaard, and S. I. Bozhevolnyi, "Metal nano-strip optical resonators," Opt. Express **15**(7), 4198–4204 (2007).
7. S. I. Bozhevolnyi, and T. Søndergaard, "General properties of slow-plasmon resonant nanostructures: nano-antennas and resonators," Opt. Express **15**(17), 10869–10877 (2007).
8. T. Søndergaard, J. Beermann, A. Boltasseva, and S. I. Bozhevolnyi, "Slow-plasmon resonant-nanostrip antennas: Analysis and demonstration," Phys. Rev. B **77**(11), 115420 (2008).
9. E. N. Economou, "Surface plasmons in thin films," Phys. Rev. **182**(2), 539–554 (1969).
10. J. Jung, T. Søndergaard, and S. Bozhevolnyi, "Gap plasmon-polariton nanoresonators: Scattering enhancement and launching of surface plasmon polaritons," Phys. Rev. B **79**(3), 035401 (2009).
11. H. T. Miyazaki, and Y. Kurokawa, "Squeezing visible light waves into a 3-nm-thick and 55-nm-long plasmon cavity," Phys. Rev. Lett. **96**(9), 097401 (2006).

#129544 - $15.00 USD Received 3 Jun 2010; accepted 20 Jun 2010; published 25 Jun 2010

12. J. Takahara, S. Yamagishi, H. Taki, A. Morimoto, and T. Kobayashi, "Guiding of a one-dimensional optical beam with nanometer diameter," Opt. Lett. **22**(7), 475–477 (1997).
13. L. Novotny, "Effective wavelength scaling for optical antennas," Phys. Rev. Lett. **98**(26), 266802 (2007).
14 H. Ditlbacher, A. Hohenau, D. Wagner, U. Kreibig, M. Rogers, F. Hofer, F. R. Aussenegg, and J. R. Krenn, "Silver nanowires as surface plasmon resonators," Phys. Rev. Lett. **95**(25), 257403 (2005).
15. G. Della Valle, T. Søndergaard, and S. I. Bozhevolnyi, "Efficient suppression of radiation damping in resonant retardation-based plasmonic structures," Phys. Rev. B **79**(11), 113410 (2009).
16. G. Della Valle, T. Søndergaard, and S. I. Bozhevolnyi, "High-Q plasmonic resonators based on metal split nanocylinders," Phys. Rev. B **80**(23), 235405 (2009).
17. F. Neubrech, T. Kolb, R. Lovrincic, G. Fahsold, A. Pucci, J. Aizpurua, T. W. Cornelius, M. E. Toimil-Molares, R. Neumann, and S. Karim, "Resonances of individual metal nanowires in the infrared," Appl. Phys. Lett. **89**(25), 253104 (2006).
18. C. Enkrich, M. Wegener, S. Linden, S. Burger, L. Zschiedrich, F. Schmidt, J. F. Zhou, Th. Koschny, and C. M. Soukoulis, "Magnetic metamaterials at telecommunication and visible frequencies," Phys. Rev. Lett. **95**(20), 203901 (2005).
19. G. Della Valle, T. Søndergaard, and S. I. Bozhevolnyi, "Plasmon-polariton nano-strip resonators: from visible to infra-red," Opt. Express **16**(10), 6867–6876 (2008).
20. G. T. Boyd, Z. H. Yu, and Y. R. Shen, "Photoinduced luminescence from the noble metals and its enhancement on roughened surfaces," Phys. Rev. B Condens. Matter **33**(12), 7923–7936 (1986).
21. M. R. Beversluis, A. Bouhelier, and L. Novotny, "Continuum generation from single gold nanostructures through near-field mediated intraband transitions," Phys. Rev. B **68**(11), 115433 (2003).
22. P. Ghenuche, S. Cherukulappurath, T. H. Taminiau, N. F. van Hulst, and R. Quidant, "Spectroscopic mode mapping of resonant plasmon nanoantennas," Phys. Rev. Lett. **101**(11), 116805 (2008).
23. P. J. Schuck, D. P. Fromm, A. Sundaramurthy, G. S. Kino, and W. E. Moerner, "Improving the mismatch between light and nanoscale objects with gold bowtie nanoantennas," Phys. Rev. Lett. **94**(1), 017402 (2005).
24. A. Hohenau, J. Krenn, F. Garcia-Vidal, S. Rodrigo, L. Martin-Moreno, J. Beermann, and S. Bozhevolnyi, "Spectroscopy and nonlinear microscopy of gold nanoparticle arrays on gold films," Phys. Rev. B **75**(8), 085104 (2007).

1. Introduction

Interaction of light with functionalized metal nanostructures is one of the main topics in the research area nano-optics [1]. This is due to the fact that excitation of plasmonic resonances in metal nanostructures leads to fascinating optical phenomena exploitable in practical applications at visible and infrared frequencies, such as guidance of electromagnetic fields beyond the diffraction limit [2], and dramatic enhancement of local and scattered electromagnetic fields that can be advantageously used for optical sensing [3]. Plasmonic resonances are typically distinguished as being either electrostatic or retardation-based. Electrostatic resonances occur due to localized collective electron oscillations in metal nanostructures having dimensions significantly smaller than the wavelength of the driving electromagnetic field and therefore subjected only to negligible retardation effects [4]. Contrary, retardation-based resonances are associated with interference of counter-propagating surface plasmon polariton (SPP) modes, i.e. electromagnetic excitations resonantly coupled to collective electron oscillations at metal/dielectric interfaces [5]. Recent studies have demonstrated that short-range SPP (SR-SPP) modes can be excited, propagate and interfere in sub-wavelength metal structures being reflected by the structure terminations [5–8]. The main property of SR-SPP modes is that they are strongly confined to the metal featuring large effective refractive indexes (ERI) with respect to that of the surrounding dielectric medium and, as a consequence, characterized with significantly reduced wavelengths. Actually, since propagating SR-SPP modes do not experience cutoff for structures with small cross sections [9], retardation-based resonances involving SR-SPP modes can indeed, similar to electrostatic resonances, exist at nanoscale [5–8]. SPP-modes not exhibiting cutoff exist in e.g. insulator-metal-insulator (IMI) [7], metal-insulator-metal (MIM) structures [7,10,11], and in nanowires [12–14], so that various configurations can be employed to facilitate efficient excitation, propagation and interference of strongly confined SPPs and, thereby, exploited in retardation-based nanoantennas.

In this paper the optical properties, in terms of scattering, extinction and field enhancement, of three-dimensional plasmonic straight nanorods being transformed into split-ring resonators by bending, are investigated by linear spectroscopy and TPL microscopy. Furthermore, optical scattering and extinction cross sections are evaluated by numerical

#129544 - $15.00 USD Received 3 Jun 2010; accepted 20 Jun 2010; published 25 Jun 2010

simulations conducted with the finite-element method (FEM). Observed changes in the scattering, extinction and field enhancement of the plasmonic nanoantennas due to structural transformations are explained by considering the SR-SPP modes forming standing-wave patterns at resonance in a way somewhat similar to that employed in recent studies of two-dimensional nano-strips being transformed into split-cylinders [15,16]. The latter observations relied, however, solely on numerical results that are rather problematic to check experimentally due to the difficulty of fabricating split-cylinders with conventional top-down fabrication techniques. Although the idea of extending this work to three dimensions increases the computational complexity required for modeling it significantly eases the fabrication process which can be conducted with electron beam lithography (EBL) and lift-off technique.

2. Design and fabrication

The plasmonic nanoantennas considered in this paper are defined by the antenna length *L*, width *w*, height *h* [Fig. 1(a)] and bending radius *R* [Fig. 1(b)]. For lengths 300nm and 400nm the nanoantenna width and height are fixed at 50nm whereas the bending radius is varied resulting in straight nanorods being transformed into split-rings by bending [Fig. 1(c)]. Two samples fabricated by EBL and lift-off is prepared in order to realize gold plasmonic nanoantennas situated on a fused silica substrate and arranged periodically with a 1µm pitch [Fig. 1(d)–1(g)] in arrays of 50x50µm^2.

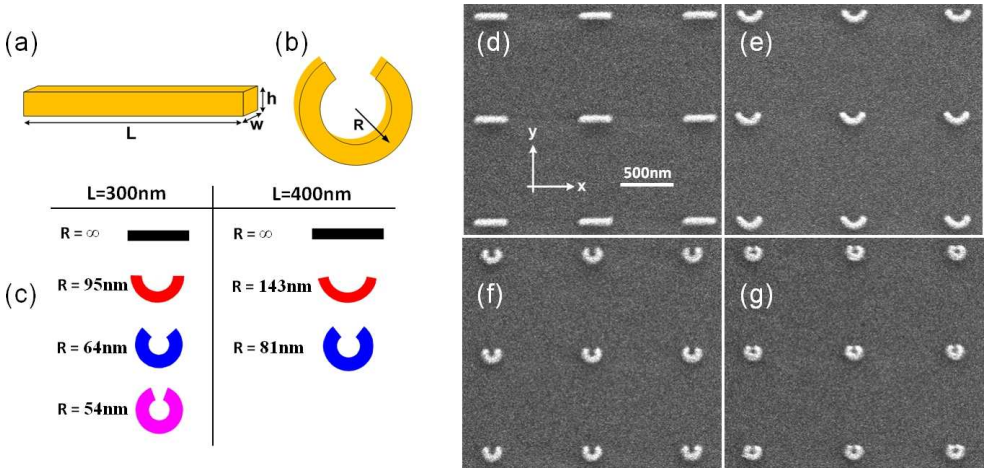

Fig. 1. (a) Dimensions of the straight nanorod with length *L*, width *w* and height *h*. (b) Split-ring obtained by bending the nanorod with a radius of curvature *R* while keeping *w* and *h* fixed. (c) Table indicating the design parameters varied for fixed width and height. (d-g) Representative scanning electron micrographs of fused silica substrates with periodically arranged gold nanoantennas with a length of 300nm and a pitch of 1µm. A charge density of 310 µC/cm^2 in the EBL exposure yielded antenna widths of ~50nm as desired.

The fabrication procedure of the two samples with antennas of lengths 300nm and 400nm, respectively, are slightly different due to the fact that bend antennas of 300nm length are more challenging to fabricate compared to those of 400nm length. In the fabrication of 300nm long nanoantennas the sample is prepared by spin coating a 4 inch fused silica wafer with the highly sensitive E-beam resist ZEP 520A 3.7% at 500rpm for 10 seconds followed by 1500rpm for 30 seconds and subsequent prebake on a hot plate for 5 minutes at 180°C yielding a resist layer thickness of ~130nm. Before E-beam exposure a ~15nm conducting thin film of aluminum is deposited thermally on top of the ZEP resist in order to prevent distorted patterns during the EBL exposure due to charge accumulation in the resist and the underlying silica substrate. Immediately after the exposure of several 50x50µm^2 arrays, carried out at 100kV acceleration voltage, 0.8nA beam current and charge densities ranging from 310 µC/cm^2 to 355 µC/cm^2 in steps of 15 µC/cm^2, the aluminum film is dissolved in

#129544 - $15.00 USD Received 3 Jun 2010; accepted 20 Jun 2010; published 25 Jun 2010

photoresist developer MF-322 and the sample rinsed with water and spin dried. Hereafter, the development of the exposed ZEP-resist is initiated by immersion into ZEP-N50 developer for 2 minutes and stopped by isopropyl alcohol (IPA) rinse followed by drying with compressed nitrogen. After E-beam deposition of ~2nm titanium at 2Å/s, in order to promote adhesion of 50nm gold deposited at 10Å/s, lift-off is carried out in an acetone bath for 10 minutes and in Remover 1165 for ~24 hours. Finally, the wafer is rinsed in acetone and IPA, dried with compressed nitrogen and cut into samples of $2x2cm^2$ with a wafer saw.

The second sample carrying nanoantennas with a length of 400nm is fabricated in more or less a similar way, except that the E-beam resist polymethyl methacrylate (PMMA) 950K (2% solids dissolved in anisole) is applied and the acceleration voltage is reduced to 30kV. The final nanoantennas did, however, exhibit widths and heights of ~60nm, i.e. ~10nm wider and higher than the antennas fabricated with a length of 300nm.

3. Scattering and extinction properties

As a first approach, linear reflection spectroscopy measurements are conducted on the nanoantennas in order to get an overview of the positions and strengths of the plasmonic resonances. Light from a broadband tungsten halogen source (~450-2000nm) is passed through a polarizer and focused onto an array of nanoantennas with an objective [x60, numerical aperture (N.A.) = 0.85]. The reflected light is collected with the same objective, passed through an analyzer and finally focused onto and collected by a VIS/NIR optical fiber connected to a spectrometer. The reflection spectra are recorded in two wavelength intervals (450-950nm and 1000-1900nm) with a VIS- and NIR spectrometer respectively, and immediately after obtaining the reflection spectrum from an array of nanoantennas a reference reflection spectrum from the silica substrate is recorded for the purpose of normalization. After subtraction of the spectrometer dark counts, the relative reflection spectrum of a specific nanoantenna array [Fig. 2(a)] is calculated as the ratio between the reflection spectrum of the nanoantennas and the reference reflection spectrum of the substrate. In the simulations, scattering and extinction cross section spectra [Fig. 2(b) and Fig. 4(b) respectively] of the corresponding modeled nanoantenna structures are normalized with respect to the geometrical surface area of the nanoantenna. In order to limit the complexity of the FEM model and the numerical load in the simulations, two approximations are incorporated in the model compared to the experimental conditions. The scattering and extinction cross sections are simulated assuming that the nanoantennas are embedded in a homogenous dielectric substrate with a refractive index of the surrounding dielectric approximated by $n_{eff} = 1.25$, which is the root mean square of the refractive indexes in air ($n_{air} = 1$) and silica ($n_{silica} = 1.45$) [17]. Experimentally, the spectra were obtained with silica below and air above the nanoantennas. Furthermore, in the simulations a plane wave (unfocused) is used as incident light, whereas a focused beam is applied when recording the experimental reflection spectra. Both approximations may slightly influence the strength and position of the simulated resonances compared to those obtained in the experiment.

#129544 - $15.00 USD Received 3 Jun 2010; accepted 20 Jun 2010; published 25 Jun 2010

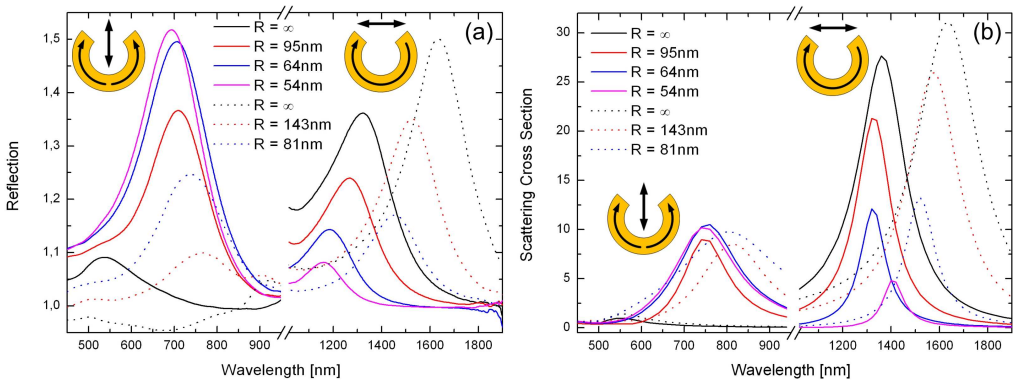

Fig. 2. (a) Experimental relative reflection spectra. (b) Simulated scattering cross section normalized to the antenna area. Spectra to the right and left of the wavelength-axis breaks are obtained with x- and y-polarization, respectively. Solid and dotted curves correspond to spectra from nanoantennas with $L = 300$nm and $L = 400$nm, respectively. The insets in (a) and (b) indicate the orientation of the electric field component as well as the plasmonic currents of the 1st order mode (right) and 2nd order mode (left) in the nanoantennas.

Resonances presented to the right- and left-hand side of the wavelength-axis breaks are recorded with x- and y-polarization of the incident light, respectively [see the orientations in Fig. 1(d) and in the insets in Fig. 2]. For x-polarization the most pronounced feature in the spectra of reflection and scattering cross section is the resonant scattering, which is increasingly suppressed when gradually decreasing the bending radius of the nanorod, i.e. when transforming the straight nanorod into a split-ring. If considering the nanoantennas as being SR-SPP resonators the enhanced scattering can be related to a resonator mode fulfilling the condition for a standing wave resonance [5]:

$$L\frac{2\pi}{\lambda_0}n_{SPP} = m\pi - \varphi \qquad (1)$$

where λ_o is the wavelength of light in free space, n_{spp} is the ERI of the SR-SPP mode, m is a positive integer representing the mode order and φ is a phase shift taking into account that the SR-SPP is not immediately reflected at the end terminations making the effective length of the nanorod larger than the geometrical length. In correspondence with Eq. (1) also a higher order mode scattering resonance (not shown in Fig. 2) was observed for shorter wavelengths (~700nm for the case of 400nm long nanoantennas) when exciting with x-polarized light. This resonance is attributed to the 3rd order mode as excitation of the 2nd order mode with x-polarization is not possible for the straight nanorod, due to symmetry mismatch between the mode field distribution and the incident field, and consequently, the resonances to the right of the wavelength-axis breaks at longer wavelengths are attributed to the 1st order mode (Fig. 2). The suppression of the 1st order mode scattering is due to the cancellation of an electric-dipole moment in ring-like structures favoring a less radiant magnetic-dipole response [15,18] stemming from partially circulating plasmonic current [see right insets in Fig. 2(a) and 2(b)].

The simulated scattering resonances with x-polarized light clearly exhibit blue-shifts for antennas with moderate bending radii, whereas antennas with bending radii equal to or smaller than 64nm actually exhibit red-shifts. Also noteworthy is the resonance linewidths which appear to narrow concurrently with decreasing bending radii. The red-shifts are due to coupling of the near-fields from the split-ring terminations [15], causing a change in the phase φ in Eq. (1), whereas the reduced linewidths are due to the suppressed electric-dipole moment and the resulting reduced radiation losses when the nanorods are bent. The experimentally recorded spectra with x-polarized light, however, only reveal blue-shifts of the scattering resonances when the bending radius is decreased, whereas red-shifts and

#129544 - $15.00 USD Received 3 Jun 2010; accepted 20 Jun 2010; published 25 Jun 2010

decreased linewidths are absent. In order to explain the contradictions between the simulated and experimental spectra it is necessary to have a closer look at the fabricated nanoantennas (Fig. 3). The curiosity of the red-shifts not being present in the experimental spectra are most likely explained by the structural imperfections induced during the E-beam exposure and caused by proximity effects resulting in a slightly broader width of the split-ring's bottom and more narrow width and smaller length of the arms [Fig. 3(c)]. First of all, if the proximity effects lead to slightly increased split-ring cross sections the confinement will be less effective and consequently n_{spp} decreases [7], which, according to Eq. (1) results in a blue-shift of the resonance wavelengths. Secondly, the resonance wavelengths are very sensitive to the coupling between the split-ring terminations so the imperfect arms may be responsible for diminished coupling explaining the absence of the red-shifts. The absent narrowing of the resonance linewidths in the reflection spectra can be reasoned by having in mind that the reflection spectra are obtained from arrays containing ~2500 structures, i.e. an ensemble, whereas the simulated scattering cross sections are obtained from individual modeled structures. Since EBL is a quasi-reproducible technique (Fig. 3), it is reasonable to assume that inhomogeneous broadening is the cause for the decreased linewidths not being revealed in the reflection spectra. In general, it is seen that the deviations between the experimental and simulated spectra increases when the bending radius decreases, and this is simply because the split-rings with small bending radii are comparably more difficult to fabricate than split-rings with larger bending radii.

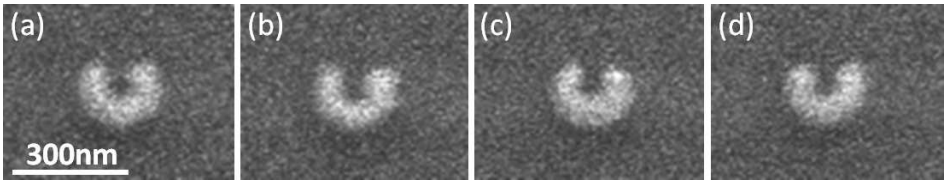

Fig. 3. Close-up of the scanning electron micrographs from Fig. 1(f) of four split-rings with bending radius 64nm. (a) Split-ring which is very similar to the design whereas (b) shows a split-ring with less bend arms, (c) increased widths in the lower part of the split-ring due to proximity effects (seen for many of the split-rings) and (d) arms of slightly different lengths.

As the polarization of the incident light is changed to the y-direction, the resonances related to the 1st order mode expectedly vanish and the resonances to the left of the wavelength-axis breaks appear. These resonances behave completely opposite compared to those of the 1st order mode as (i) the scattering strength increases when the bending radius is reduced and (ii) the spectral positions of the resonances are quite insensitive to the bending radius. In the limit where the bending radius reaches infinity, scattering resonances are either completely suppressed (Fig. 2, black dotted curves) or very weak (Fig. 2, black solid curves). These characteristics are actually expected since y-polarization contrary to x-polarization of the light allows efficient excitation of the 2nd order mode comprised of excited electric dipoles in the two arms of the split-rings, however, only when bending has been introduced [left insets in Fig. 2(a), 2(b)]. Therefore, by controlling the bending radius the scattering strength of the 1st and 2nd order mode can be modified, though not independently. The fact that the resonance wavelength of the 2nd order mode is quite insensitive to the bending radius is most likely ascribed to negligible coupling between the split-ring terminations for this mode as our simulations show that the 1st order mode has a large part of its energy concentrated at the antenna terminations (see also [15]), thereby exhibiting increased near-field interactions for small radii of curvature, whereas the 2nd order mode has an insignificant amount of energy concentrated at the antenna terminations. Also, the strength of the 2nd order mode relative to that of the 1st order mode is actually larger in the experiment for the nanoantennas of length 300nm, another feature not observed in the simulated scattering cross sections. However, as mentioned this may be ascribed to the different principles of illumination in the experiment and simulations.

#129544 - $15.00 USD Received 3 Jun 2010; accepted 20 Jun 2010; published 25 Jun 2010

The weak scattering peak, observed for straight nanorods at ~530nm [Fig. 2(a)], is indicating that it is possible to excite an electrostatic resonance when applying y-polarization. The strength of this electrostatic resonance is quite small compared to the observed retardation-based resonances, but this is due to a comparably smaller electric-dipole response contributing to scattering in the far field when exciting with a polarization of the electric field component along the short axis of the nanorods. Finally, another important feature is that all the resonances seen in the spectra are blue-shifted when the nanoantenna length is decreased from 400nm to 300nm, which is in complete accordance with Eq. (1), and therefore may be tailored by the same scaling principles as demonstrated for nano-strips [8,19]. These observations are of great importance since they strongly support our assumptions of retardation-based SR-SPP resonances being excited in nanoantennas and thereby forming standing waves due to constructively interfering counter-propagating SR-SPPs.

In an identical approach, linear transmission spectroscopy and FEM modeling is employed to obtain experimental [Fig. 4(a)] and simulated [Fig. 4(b)] extinction spectra of the nanoantennas and the spectra also reveal excitation of the 1st and 2nd order modes. The experimental extinction setup is similar to the one used for reflection except that an unfocused beam of white light is used for illumination through the sample, i.e. more similar to the modeled illumination in the simulations.

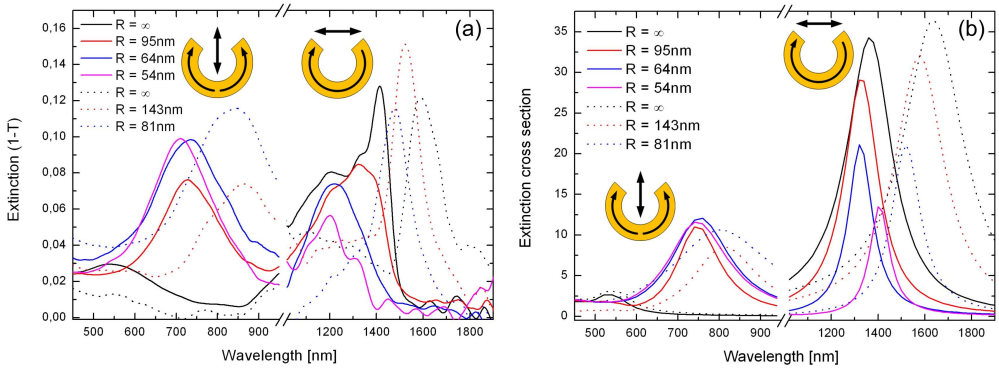

Fig. 4. (a) Experimentally obtained extinction spectra. (b) Simulated extinction cross section normalized to the antenna area and the energy of the incident plane wave. Spectra to the right and left of the wavelength axis break are obtained with x- and y-polarized light, respectively. Solid lines correspond to spectra obtained from antennas with L = 300nm and dotted lines are spectra obtained from antennas with L = 400nm. The insets in (a) and (b) indicate the orientation of the electric field component as well as the plasmonic currents of the 1st order mode (right) and 2nd order mode (left) in the antennas.

Overall, the trends seen in the extinction spectra are the same as in the reflection spectra, but in the case of extinction absorption is also included which is why the level of extinction is slightly larger than that of pure scattering [Fig. 2(b) and Fig. 4(b)]. However, there is one notable characteristic in the measured extinction spectra, the extinction resonance of the 1st order mode for the split-ring of length 400nm and bending radius 143nm being slightly stronger than the corresponding straight nanorod resonance [Fig. 4(a), red dotted curve to the right]. This unexpected feature is not seen in any of the other measured or simulated spectra, and is therefore physically difficult to explain. Notice also that the relative strengths of the 1st and 2nd order modes in the experimental extinction spectra are different from those in the experimental reflection spectra, most likely due to the different principles of illumination. Despite a few discrepancies the agreement between the experimental and simulated spectra are quite good and has provided an overview of the resonant wavelengths and strengths for the fabricated nanoantennas.

#129544 - $15.00 USD
Received 3 Jun 2010; accepted 20 Jun 2010; published 25 Jun 2010

4. TPL microscopy and local field enhancement

The second approach for probing the resonant behavior of the nanoantennas is by nonlinear scanning optical TPL microscopy. TPL from metals is a well known nonlinear optical phenomenon [20], and spatially resolved TPL measurements have shown to be suitable for characterization of local field enhancement in plasmonic nanostructures [21,22]. Especially, TPL is attractive as a probe for local field enhancement since TPL is quadratically dependent on the power of the local electric field, making the technique extremely sensitive to intense electric fields [20].

The experimental setup [Fig. 5(a)] consists of a scanning optical microscope, operated in reflection geometry, and the scanning is computer-controlled by a translation stage which steps down to 50nm (accuracy ~4nm). Linearly polarized light from a pulsating mode locked Ti-Sapphire laser with ~200fs pulse duration and ~80MHz repetition rate is used for illumination of the sample with the fundamental harmonic (FH) wavelengths ranging from approximately 720nm to 850nm, i.e. wavelengths coinciding with the resonances of the 2nd order mode. The beam of the Ti-Sapphire laser is guided through an optical isolator (OI), half-wave plate (λ/2), polarizer (P), red colour filter (F1) and wavelength selective beam splitter (WSBS) and finally focused onto the sample (S) with a Mitutoyo infinity-corrected (x100, N.A. = 0.70) objective (L). The half-wave plate and polarizer enables precise adjustment of the FH incident light power. The generated TPL radiation and the reflected FH beam are concurrently collected with the same objective, separated by the WSBS, directed through a red- and blue (F2) color filter, respectively, and finally detected with the two photomultiplier tubes (PMTs). Furthermore, the PMT for detection of the TPL signal is connected to a photon counter giving typically ~20 dark counts per second (cps).

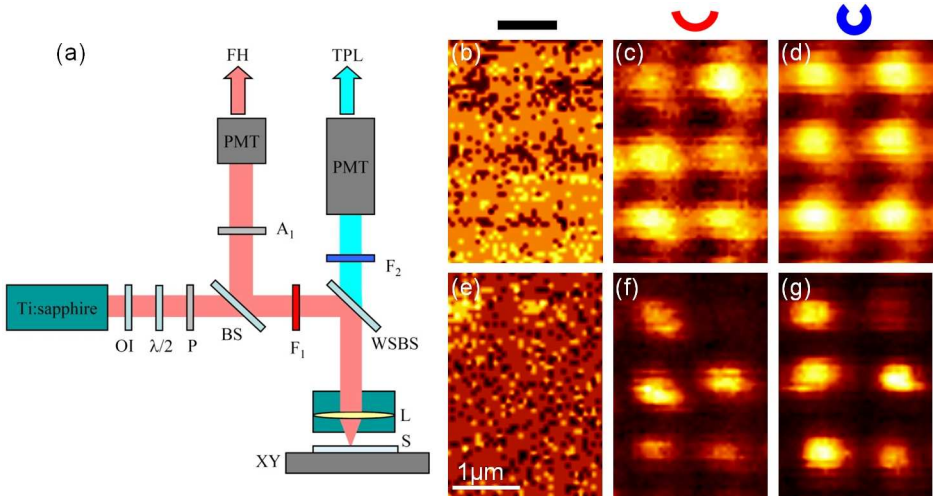

Fig. 5. (a) Illustration of the experimental setup for nonlinear scanning optical microscopy operated in reflection with a Ti-Sapphire laser, optical isolator (OI), half-wave plate (λ/2), polarizer (P), beam splitter (BS), filters F_1 and F_2, wavelength selective beam splitter (WSBS), objective (L), sample (S) placed on a XY-table, analyzer A_1, and photomultiplier tubes (PMTs). (b-d) FH and (e-g) corresponding TPL images of six nanoantennas with a length of 400nm and infinite, 143nm and 81nm bending radius respectively obtained with y-polarized light at λ = 750nm and incident power ~0.15mW. The average TPL signal from the six nanoantennas is (e) ~11, (f) ~211 and (g) ~460cps.

The FH wavelength of 750nm coincides well with the scattering resonances of the antennas with a length of 400nm [Fig. 2(a)], and the distinction between the resonances, when transforming the straight nanorods to split-rings, is appreciable. Therefore, as a first experiment, FH [Fig. 5(b)–5(d)] and TPL images [Fig. 5(e)–5(g)] of six nanoantennas with a length of 400nm and geometry of straight nanorods [Fig. 5(b), 5(e)] and split-rings with

#129544 - $15.00 USD
Received 3 Jun 2010; accepted 20 Jun 2010; published 25 Jun 2010

bending radii 143nm [Fig. (c,f)] and 81nm [Fig. (d,g)] are obtained with y-polarized light for a fixed wavelength of 750nm and incident power of ~0.15mW. The recorded images verify the efficient excitation of the 2nd order mode resonance as soon as the straight nanorods are transformed into split-rings since both the FH- and TPL intensities increase concurrently with decrease in the bending radius. Actually, it was impossible to image the straight nanorods when using only ~0.15mW of incident power, whereas the periodic bright spots from the split-rings immediately appeared in the TPL image. The average TPL signal generated from the six nanoantennas (after subtracting dark counts) increased from ~11 cps for straight nanorods to ~211 and ~460 cps for split-rings with bending radii 143nm and 81nm respectively verifying that the strength of the 2nd order resonance is very sensitive to the bending radius as signified by the linear reflection- and extinction spectra. The somewhat inhomogeneous appearance of bright spots [Fig. 5(f), 5(g)] were characteristic for all the TPL images indicating that the local enhanced fields are very sensitive to minor structural variations which, as discussed when explaining the deviations of the experimental from the simulated linear spectra, are certainly present (Fig. 3).

So far it has been demonstrated that the TPL signal level, and therefore the local field enhancement, is sensitive to the bending radius of the nanoantenna due to changes in the excitation efficiency of the 2nd order mode. In order to further verify the observed wavelength dependence of the 2nd order mode resonance seen in the reflection- and extinction spectra, the average intensity enhancement factors α are estimated from TPL-images recorded at different FH-wavelengths. However, before choosing an appropriate FH wavelength interval on the basis of the reflection and extinction spectra, it should be noted that the 2nd order mode resonance wavelength for a specific 400nm long nanoantenna deviate by ~75nm depending on whether the resonance wavelength is inferred from the reflection or extinction spectrum [Fig. 2(a) and Fig. 4(a)]. This deviation is, as previously mentioned, attributable to the diverse principle of illumination in reflection- and extinction measurements, respectively. Given that the nanoantennas are also excited with a focused beam in the TPL measurements, the wavelengths of the incident light is, on the basis of the reflection spectra, chosen in the interval 750-850nm in steps of 20nm. For each FH wavelength several TPL images of the same six nanoantennas are recorded for each of the three different types of nanoantennas with length 400nm in order to investigate the wavelength dependence of the 2nd order mode resonance. From these images the average intensity enhancement factor α of the six nanoantennas, when taking the surface area and incident power generating the TPL signal into account, is estimated by using the relation [23,24]:

$$\alpha = \sqrt{\frac{\langle TPL_{na} \rangle \langle P_{gold} \rangle^2 A_{gold}}{\langle TPL_{gold} \rangle \langle P_{na} \rangle^2 A_{na}}} \tag{2}$$

where the sub-indexes gold and na refer to a smooth gold reference surface and nanoantenna structure, respectively, $\langle TPL \rangle$ is the time-averaged (100ms) TPL signals when the focus spot (diameter ~0.75μm) of the Ti-Sapphire laser is centered either on the nanoantenna or smooth gold film respectively, $\langle P \rangle$ is the averaged incident power that yields $\langle TPL \rangle$ and A is the surface area from which $\langle TPL \rangle$ is generated. A smooth gold film of 50nm thickness is used as reference and the deposition is performed with similar pressure and rate parameters as are used for fabrication of the nanoantennas. The estimated intensity enhancement factors versus the FH wavelength (Fig. 6) reproduces the trends for the 2nd order mode seen in the reflection spectra [Fig. 2(a)] quite well. The reflection spectra as well as the enhancement curves indicate that the strength of the resonance at approximately 750nm is diminished at larger split-ring bending radius and both quantities decrease when tuning the FH wavelength

#129544 - $15.00 USD Received 3 Jun 2010; accepted 20 Jun 2010; published 25 Jun 2010

on the long-wavelength side of the reflection resonance. The influence of the detuning is most significantly observed for the split-rings with 81nm bending radius.

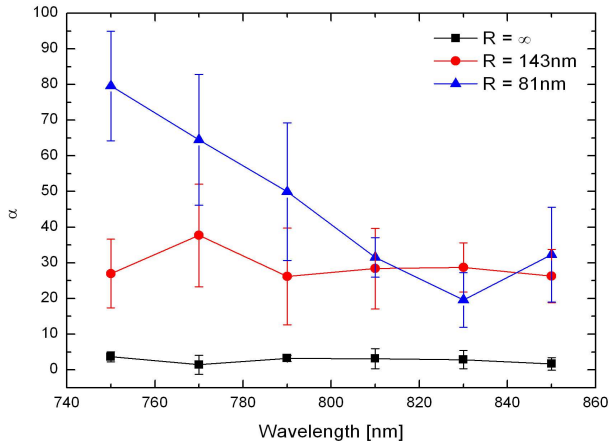

Fig. 6. Intensity enhancement factor α versus the FH wavelength for straight nanorods and split-rings with bending radii 143nm and 81nm. Each point on the curves indicates the average intensity enhancement from six nanoantennas and the error bars indicate the standard deviation of these measurements.

The TPL studies demonstrate resonant excitation of the 2nd order mode leading to enhancement factors up to ~80 when averaging the enhancement from six nanoantennas. As already discussed the TPL signal and therefore also α is very sensitive to minor structural imperfections, which is why the standard deviations increase when the bending radius decreases. Nevertheless, the distinction in the intensity enhancement for the three different nanoantennas is still appreciable when taking the standard deviations into account.

5. Conclusion

In conclusion, we have investigated resonant scattering and extinction as well as local field enhancement factors by plasmonic nanoantennas when being transformed from straight nanorods to split-rings. It has been demonstrated that SR-SPP modes forming standing waves dominate the scattering and extinction spectra, and that the resonant scattering- and extinction strengths can be modified by changing the bending radius of nanoantennas. Importantly, the scattering- and extinction resonances of the 1st order mode were shown to be strongly suppressed when bending straight nanorods, a behavior that is attributed to the decrease in the nanoantenna electric-dipole response. Conversely, we demonstrated that the scattering- and extinction resonances of the 2nd order mode are enhanced when decreasing the bending radius due to the emerging electric-dipole response from the two arms of nanoantennas. Furthermore, the experimental observations were corroborated with and confirmed by numerical simulations that reproduce quite well the tendencies seen in the linear spectra. TPL measurements from 400-nm-long nanoantennas demonstrate a maximum average intensity enhancement of ~80 when resonantly exciting the 2nd order mode with y-polarized light, verifying also to a great extent the trends seen in the reflection- and extinction spectra for the 2nd order mode. Finally, the multiple resonant response in terms of scattering and extinction as well as the accessible local field enhancement makes the split-rings promising candidates for sensing at visible and near-infrared frequencies.

#129544 - $15.00 USD Received 3 Jun 2010; accepted 20 Jun 2010; published 25 Jun 2010